Available online at www.sciencedirect.com
ScienceDirect
Journal of the European Ceramic Society 27 (2007) 4665–4673
www.elsevier.com/locate/jeurceramsoc

Hematite nucleation and growth in the firing of carbonate-rich clay for pottery production

L. Nodari [a,b,*], E. Marcuz [a], L. Maritan [c], C. Mazzoli [c,d], U. Russo [a,b]

[a] *Dipartimento di Scienze Chimiche, Università di Padova, Via Marzolo 1, I-35135 Padova, Italy*
[b] *Padova Research Unit, INSTM Consortium, Padova, Italy*
[c] *Dipartimento di Geoscienze, Università di Padova, Via Giotto 1, I-35121 Padova, Italy*
[d] *Istituto di Geoscienze e Georisorse, CNR – Padova, Corso Garibaldi 37, I-35121 Padova, Italy*

Received 22 November 2006; received in revised form 14 March 2007; accepted 25 March 2007
Available online 4 June 2007

Abstract

Here we describe the evolution of iron-bearing phases in the firing of carbonate-rich illite and chlorite clay. Breakdown of chlorite forms an amorphous phase, which continues to retain iron in a (distorted) paramagnetic octahedral site, until carbonates start to decompose and react at 750 °C, forming Ca-silicates. Only at this temperature can hematite nucleate and grow in specific micro-domains located in former chlorite flakes. At 950 °C, decomposition of illite in the presence of an amorphous phase and CaO produces a melt in which nano-sized hematite may nucleate, although its growth is inhibited due to low diffusion with respect to soaking time.

Keywords: Firing; Grain growth; Grain size; Mössbauer spectroscopy; Traditional ceramics

1. Introduction

Gibbs' Phase Rule predicts that the maximum number of phases simultaneously at equilibrium – i.e., in invariant conditions – cannot exceed the number of components plus two, although it is generally lower. At constant values of the intensive variables, various mineral assemblages may form, starting from different bulk compositions. Therefore, in systems characterised by sluggish diffusion for given components – e.g., with respect to heating rate and soaking time – compositional differences from site to site may constitute microdomains within which local equilibria produce varying mineral assemblages. The addition of one chemical component to such a system may considerably increase the number of possible mineral assemblages in each microdomain. For example, at high temperatures, the firing of carbonate-rich clay for pottery production has been observed to produce a large number of mineral phases with respect to carbonate-poor clay,[1,2] due to control of local equilibria and irreversible reactions on the formation of stable mineral assemblages. At appropriate temperatures, the decomposition of calcite in the presence of quartz and clay minerals may lead to the crystallisation of diopside, melilite, wollastonite, K-feldspar, anorthite, and usually also hematite.[3,4] Duminuco et al.[3] also argued that decomposition of calcite produces a fluid phase, which enhances reaction kinetics and diffusion.

The effects of carbonate on the firing of ceramics have been thoroughly discussed by several authors [5–7,1,8–10] in terms of both sequence of reactions and textural modifications during firing.[11,6,3,1] The presence of carbonate with appropriate grain-size improves the mechanical properties of pottery in comparison with carbonate-free starting raw materials over a wide range of firing temperatures (800–1000 °C), both as regards the high stability of Ca-silicates forming during firing and the early formation of a glassy phase.[10,12] The decomposition of carbonate may also produce secondary porosity, which increases thermal diffusion and enhances the properties of pottery such as cooking ware, although the related higher water absorption results in lower quality when bricks are produced.[9,10]

The total amount of iron in the raw material and redox conditions of firing are generally the main factors determining the colour of potsherds. Carbonate-free clays tend to produce reddish-brown pottery when fired in an oxidising atmosphere, and become dark grey to black in a reducing atmosphere.[13,14]

* Corresponding author at: Dipartimento di Scienze Chimiche, Università di Padova, Via Marzolo 1, I-35135 Padova, Italy. Tel.: +39 049 8275321; fax: +39 049 8275161.
E-mail address: luca.nodari@unipd.it (L. Nodari).

0955-2219/$ – see front matter © 2007 Elsevier Ltd. All rights reserved.
doi:10.1016/j.jeurceramsoc.2007.03.031

When carbonate-rich clays are fired in the same firing conditions, pottery with creamy or brownish colours is produced.[15] In oxidising firing conditions and at an adequate temperature, hematite commonly forms, and is the main pigmenting mineral phase in potsherds, whether carbonate is present in the starting clay or not. In carbonate-free systems, the total amount of hematite increases with increasing firing temperature, at the expense of other oxides and oxyhydroxides in the raw clay, and/or as a consequence of progressive decomposition of silicates, which bear structural iron. In the case of carbonate-rich clay – i.e., with CaO derived from carbonates greater than 5 wt% – Maniatis et al.[16] observed a significant decrease in hematite content at firing temperatures between 900 and 1080 °C, and argued that the growth of calcium silicates may inhibit the crystallisation of hematite, favouring the formation of poorly crystallised new oxides, possibly with Al substitution, and lowering the magnetic component over the total absorption ratio in Mössbauer spectra. Mackenzie[17] and Wagner and Wagner[18] also invoked the solution of iron into the calcium silicate lattice with increasing temperature, leaving less iron as oxides. A multi-analytical approach was adopted here, in order to verify some of these speculations and to understand fully the decomposition, nucleation, grain-size and microstructural location of iron phases during firing in a carbonate-rich illitic-chloritic clay. This specific bulk mineral composition was chosen considering that such a starting clayey material has a wide geographic distribution in temperate regions, is extensively exploited for the production of construction materials and pottery, and was commonly used for pottery production in historical and pre-historical times. Knowledge of the changes occurring during firing and their influence on several macroscopic features such as hardness, colour and heat conductivity, gives information on the degree of awareness of ancient potters in selecting specific clayey materials for their production.

2. Experimental procedure

A naturally occurring clay relatively rich in Fe_2O_{3tot} (7.25 wt%) and CaO (9.73 wt%), and characterised by a high Fe_2O_{3tot}/CaO ratio (0.745), was collected in the countryside north-west of Este (south of the Euganean Hills, north-eastern Italy) and used *tout court* in a set of firing experiments.

The chemical composition of the starting clay was determined by X-ray fluorescence (XRF) spectroscopy, on a Philips PW 2400 spectrometer, equipped with a Rh tube, preparing the sample as a bead of calcined powder and $Li_2B_4O_7$, with a dilution ratio of 1:10, and applying geological standards for calibration. FeO content was determined by titration with potassium permanganate, and compared with the FeO/Fe_2O_3 ratio obtained from Mössbauer spectroscopy. Thermo-Gravimetric (TGA) and Differential Thermal Analyses (DTA) were also performed on the clay, with custom-built equipment, by heating the sample to 1000 °C in an oxidizing atmosphere at a heating rate of 10 °C/min.

The clay was then prepared in 5 cm × 1.5 cm discs, dried at room temperature for 7 days and then at 50 °C in an oven for 24 h, and finally submitted to firing temperatures (T_f) from 300 to 1100 °C, in successive temperature steps of 50 °C, in air ($fO_2 \sim 0.2$ bars) at a heating rate of 200 °C/h, soaking time of 6 h, and cooling rate of 50 °C/h, in a MT furnace equipped with a digital microprocessor (Digitronik DCP200, Yamateke-Honeywell) for the control of firing curves. The mineral composition of both the fired samples and the staring clay was determined by X-ray diffraction (XRD) on a Philips PW 3710 diffractometer with Cu Kα radiation. Fourier Transform Infrared (FT-IR) spectroscopy was also applied, with a Nicolet FT-IR spectrometer equipped with a DTGS detector, dispersing the samples in anhydrous KBr (Aldrich, 99+%) at a dilution ratio of 1:100. Spectra were collected in the range from 4000 to 400 cm^{-1}, running 128 scans at a 4 cm^{-1} resolution for each spectrum. When necessary, the second derivative method was used to resolve overlapping absorptions. All samples were also studied by Mössbauer spectroscopy on a conventional constant-acceleration spectrometer equipped with a room-temperature Rh matrix ^{57}Co source. All spectra were collected at room temperature (RT) and at liquid nitrogen temperature (80 K), in a liquid nitrogen static cryostat. The hyperfine parameter isomer shift (IS), quadrupole splitting (QS), full linewidth at half maximum (W), expressed in mm/s, and the internal magnetic field (H_{int}), expressed in Tesla, were obtained by means of a standard least-squares minimisation technique. The spectra were fitted to Lorentzian line shapes using a minimum number of sextets and doublets. The IS is quoted relative to metallic iron at room temperature. When necessary, 10 K spectra were also collected on an ARS® close circuit cryostat.

We assume that, in all spectra, the hyperfine parameters were affected by the same error, postulated as the maximum error over all measurements. We assigned ±0.03 mm/s to isomer shift, ±0.03 mm/s to quadrupole splitting (or quadrupole shift for magnetically split components), ±0.03 mm/s to linewidth, ±0.1 T to hyperfine magnetic field, and ±2% to relative area. Following the suggestion of Oh and Cook,[19] we also assumed that the recoilless fraction (f) for hematite is the same at both room and low temperature. This assumption is supported by the observation that the 80 K and 10 K spectra are not significantly different.

On selected samples – unfired starting clay, and samples fired at 750 °C, 850 °C, 950 °C and 1050 °C, respectively – dithionite soluble iron was chemically separated following the procedure described by Mehra and Jackson.[20] The supernatant solution was diluted to 100 ml in deionised water and then analysed by inductively coupled argon plasma optical emission spectrometry (ICP-OES) at the Dipartimento di Ingegneria Meccanica (University of Padova) on a Spectro Flame SOPS/N6410/95A. For Fe determination, the 2% $Fe(NO_3)_3 \cdot 9H_2O$ in HNO_3 standard (BDH Chemical Ltd.) was used, and for Al determination, a 2% $Al(NO_3)_3 \cdot 9H_2O$ in HNO_3 (EXAXOL Italia S.r.l.).

3. Results

3.1. Raw clay material

The starting clay was naturally composed by a carbonate-rich fraction with a grain size from clay to silt, and a few coarser

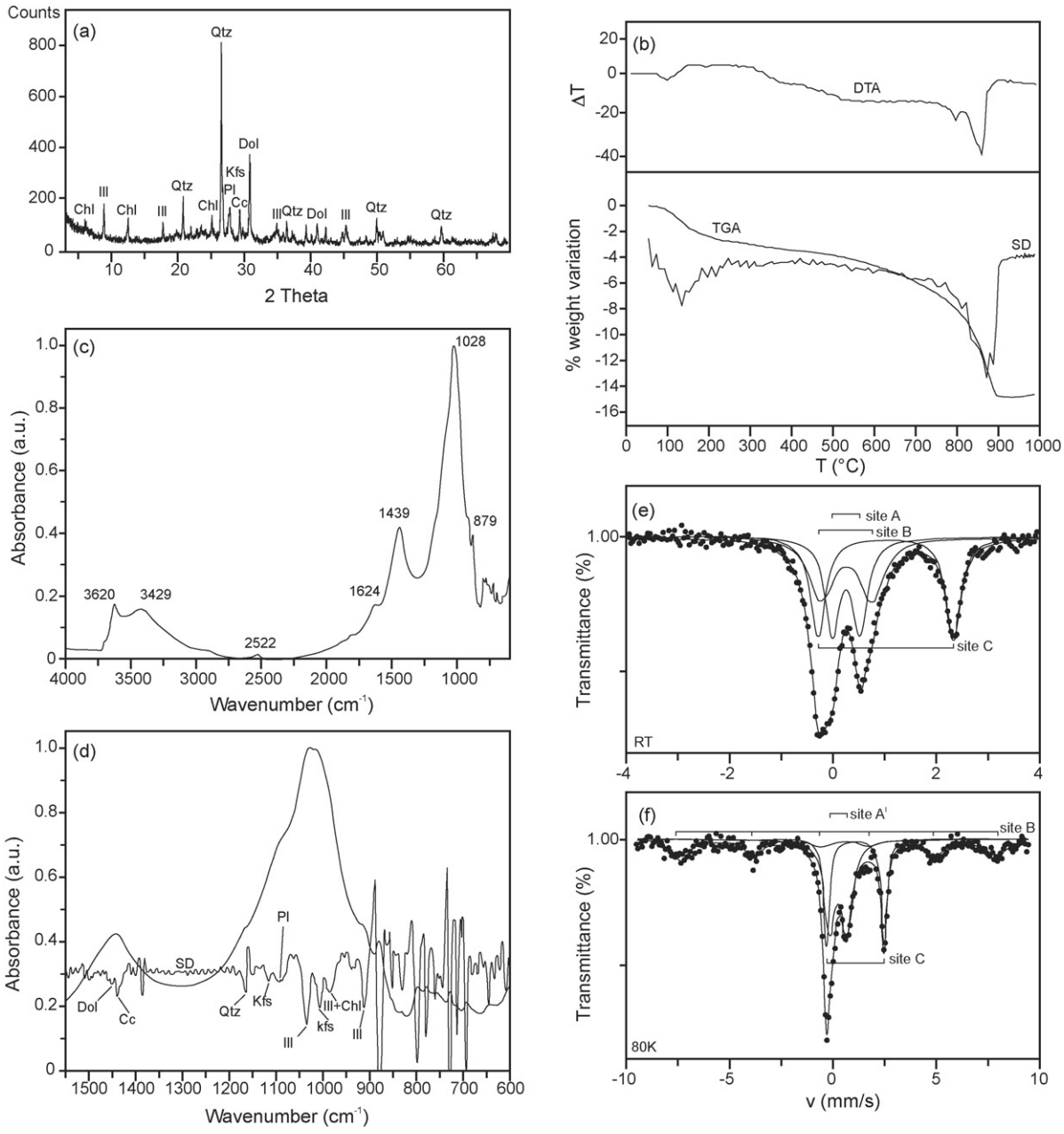

Fig. 1. (a) XRD pattern, (b) differential thermal (DTA), thermo-gravimetric (TGA) and second derivative (SD) diagrams, (c) complete FT-IR spectrum and (d) detail of 1500–900 cm^{-1} wavenumber region and relative second derivative, (e) room temperature (RT) and (f) 80 K Mössbauer spectra for starting clay. Mineral abbreviations: Ill: illite; Chl: chlorite; Qtz: quartz; Pl: plagioclase; Kfs: K-feldspar; Cc: calcite; Dol: dolomite.

grains of quartz, illite and micritic limestone up to 0.1 mm in size, and had the following chemical composition (expressed in wt%): SiO_2 (53.37), TiO_2 (0.82), Al_2O_3 (17.31), Fe_2O_3 (4.68), FeO (2.31), MnO (0.15), MgO (6.15), CaO (9.73), Na_2O (1.42), K_2O (3.32), P_2O_5 (0.20), with a loss on ignition of 15.08 wt%. Starting mineral assemblage was determined by XRD (Fig. 1a) and illite, chlorite, quartz, calcite, dolomite, plagioclase and K-feldspar were identified. Some of these mineral phases were also identified by DTA and TGA (Fig. 1b) by comparison with data from the literature.[21,22] In particular, the endothermic peak at 130 °C and the inflexion point around 200 °C in the DTA pattern (Fig. 1b) were attributed to the removal of hygroscopic water from illite, the continuous loss of weight between 550 and 700 °C to that of chlorite, and the two endothermic peaks at 800 °C and 850 °C, and the associated loss of weight, were related to decarbonation of dolomite (15 wt%) and calcite (7 wt%), respectively. The FT-IR spectra and relative second derivative patterns (Fig. 1c and d) further confirm XRD, DTA and TGA data. The RT Mössbauer spectrum shows the typical pattern of a silicate mixture, characterised by strong absorption at low velocity, due to paramagnetic iron. The best fit of the spectrum was achieved using a model with three subspectra, referring to two octahedral Fe(III) (sites A and B) and one octahedral Fe(II) (site C which, from a crystallographic point of view, may coincide with sites

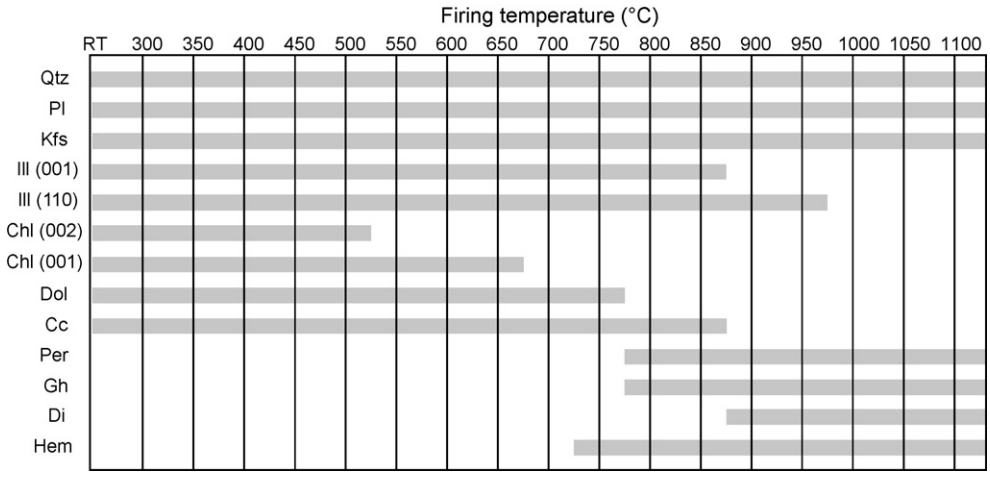

Fig. 2. Bar-diagram showing variations in mineral assemblages with increasing firing temperature. Per: periclase; Gh: gehlenite; Di: diopside; Hem: hematite. Other abbreviations as in Fig. 1. *hkl* indexes in brackets.

A or B) (Fig. 1e), 65% of total iron being accommodated in the Fe(III) sites and the remaining 35% in the Fe(II) site.

After cooling the system to 80 K, the typical sextet of magnetic absorption became evident (Fig. 1f), related to the superparamagnetic behaviour of nano-sized oxide/oxyhydroxide particles. Mössbauer parameters were typical of poorly crystalline and/or Al-substituted goethite (α-FeOOH).[18] The best fit of the 80 K spectrum was achieved considering two paramagnetic components – Fe(III) in site A' and Fe(II) in site C – and one magnetic component. In applying this model, we assumed that the two RT paramagnetic ferric sites A and B overlapped in the single 80 K site A', which turns out to be representative of the whole Fe(III) paramagnetic contribution. The broad shape of the sextet and the related magnetic parameters (IS: 0.45 mm/s; QS: −0.27 mm/s, *W*: 0.85 mm/s; *H*: 51.7 T) are characteristic of an Al-substituted and/or poorly crystalline goethite. No further superparamagnetic components were identified from the spectrum at 10 K. According to Murad and Johnston,[23] spectra already blocked at 80 K are compatible with goethite particles about 20 nm in size. Small differences in the ferrous site area – i.e., 28% at RT *versus* 20% at 80 K – may derive from small variations in the recoilless fraction, which is not always strictly constant.

3.2. Fired clay samples

The mineral assemblages in the fired clay samples were determined by XRD. Results are shown in the bar-diagram of Fig. 2. The first variations in the mineral assemblage with respect to the starting clay occurred between 500 and 650 °C, with the progressive decomposition of chlorite, marked by disappearance of the (0 0 2) and (0 0 1) reflections, and between 700 and 750 °C, when hematite started to form, or at least its modal fraction increased above the XRD detection limit. The decomposition of dolomite and calcite occurred at about 750–800 °C and 800–850 °C respectively, temperatures which are about 50 °C lower than those observed in DTA (Fig. 1b). A possible explanation for this discrepancy is the lower residence time in DTA, causing a greater deviation from equilibrium.[13] The decomposition of carbonates

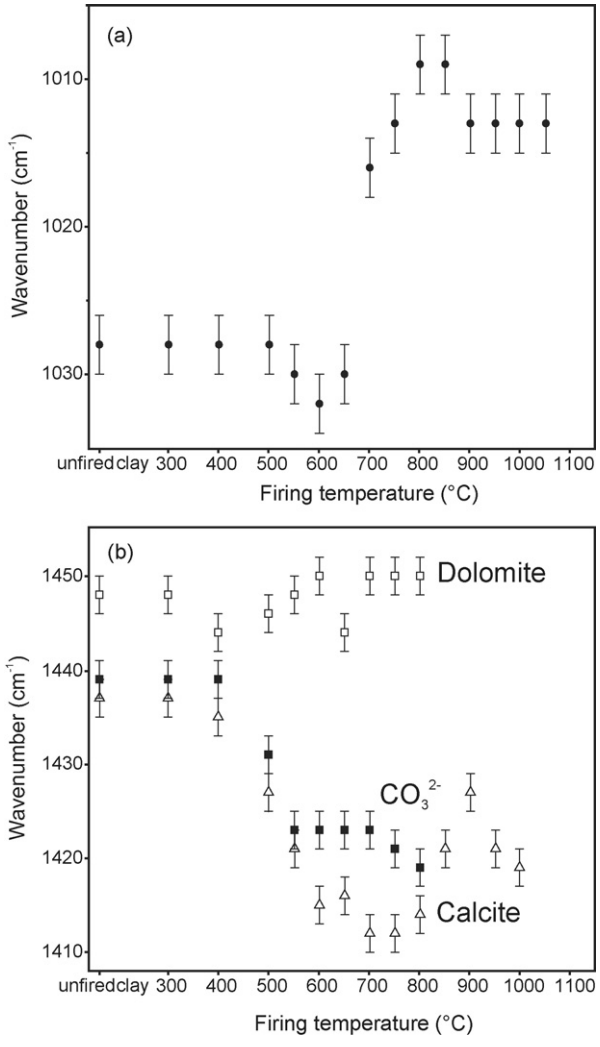

Fig. 3. Wavenumber *vs.* firing temperature for (a) Si—O and (b) CO_3^{2-} stretching bands. Filled symbols: peaks in FT-IR spectra; open symbols: calcite and dolomite peaks in second derivative pattern.

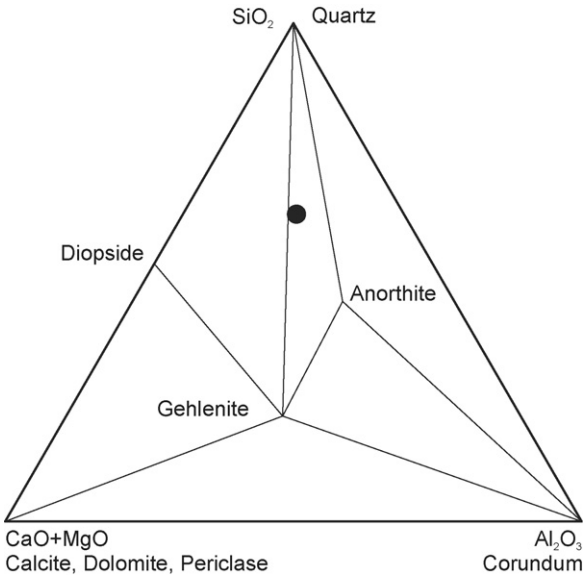

Fig. 4. Al_2O_3–(CaO + MgO)–SiO_2 (ACS) diagram. Circle: projection of chemical composition of clay material used for firing experiments.

and reaction of products with the mineral phases in the surrounding matrix caused the growth of periclase (MgO), gehlenite ($Ca_2Al_2SiO_7$) and diopside ($Ca(Mg,Fe)Si_2O_6$). Lastly, the gradual decomposition of illite between 850 and 1000 °C was marked by the progressive disappearance of the (0 0 1) and (1 1 0) peaks. In addition, the intensity of the diffraction patterns of plagioclase and K-feldspar progressively increased with increasing temperature, suggesting the occurrence of continuous reactions between illite and calcite, and between gehlenite and quartz, respectively, as well as an increase in amorphous matter.[24,6,3,13]

Reactions involving silicates in the 700–900 °C temperature range also caused progressive broadening of the Si–O stretching band and shift of the band centre, which at low temperature is located at about 1028 cm^{-1}, in the mid-region of the FT-IR spectra (Fig. 3a). Further broadening of this band above 900 °C suggests the formation of glass.[25] At the same time, typical signals of K-feldspar (1013 cm^{-1}), diopside (977 cm^{-1}) and gehlenite (935 cm^{-1}) progressively increased in intensity. The second derivative of the absorption band in the typical infrared region for carbonates showed that the peak at 1437 cm^{-1} in raw material derives from the contribution of both calcite and dolomite (Fig. 1d). On increasing T_f, the band centre progressively shifted towards smaller wavenumbers and became less intense (Fig. 3b). FT-IR data show that dolomite was completely decomposed at $T_f > 800$ °C (Fig. 3b), in agreement with the literature.[26] The FT-IR spectra of samples fired at higher T_f only showed the signal of calcite, which apparently persisted in small quantities above decomposition temperature – in the interval 830–870 °C, according to Boynton[27] – although not detected in the XRD patterns. Shoval[28] attributed the presence of calcite in high temperature spectra to recarbonation during cooling. Maritan et al.[29] argued that the weak CO_3^{2-} stretching peak above the calcite decomposition temperature is related to crystallisation of calcite after portlandite, which may derive from free CaO available for hydration after firing. The CO_3^{2-} stretching band of

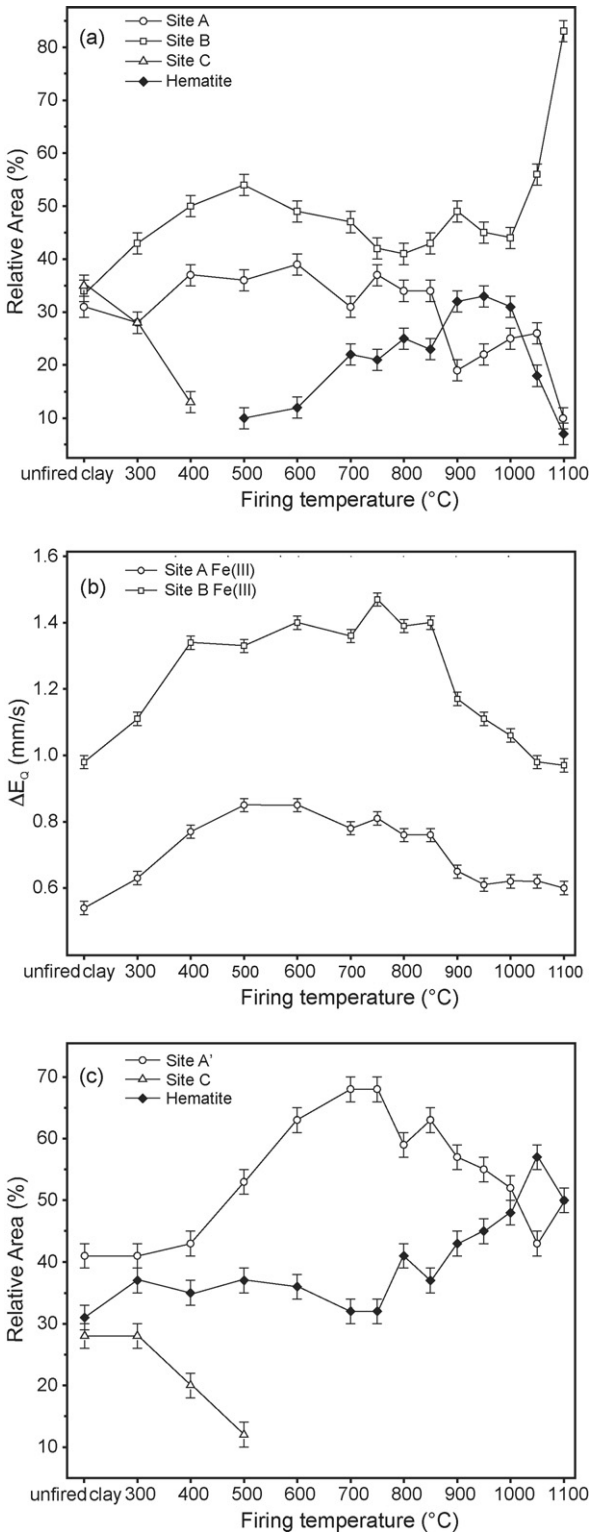

Fig. 5. Mössbauer hyperfine parameters *vs.* firing temperature: (a) RT relative areas; (b) RT quadrupole splitting; (c) 80 K relative areas.

calcite in the starting clay was located at about 1437 cm^{-1}, and persisted unchanged in the spectra of samples fired up to 400 °C. Between 400 and 600 °C, the stretching band of calcite progressively shifted towards a wavenumber of 1417 cm^{-1}, which is more similar to what was expected for well-crystallised calcite.

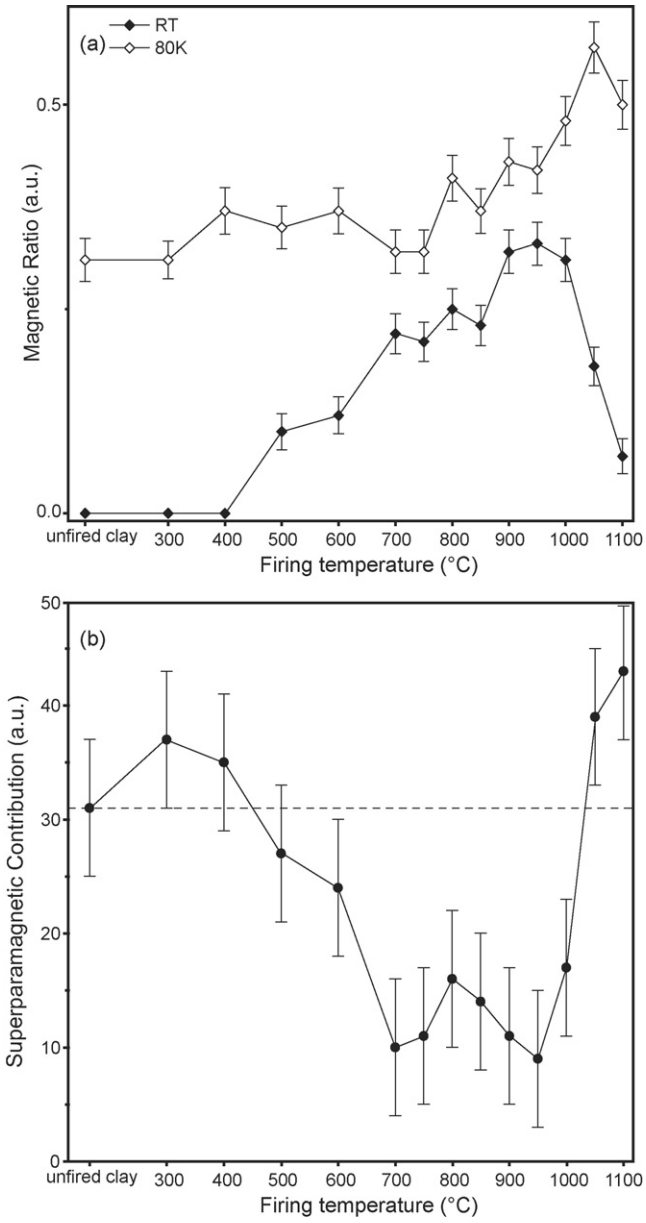

Fig. 6. (a) Magnetic ratio *vs.* firing temperature; (b) superparamagnetic contribution *vs.* firing temperature. Dashed line: superparamagnetic contribution in starting clay.

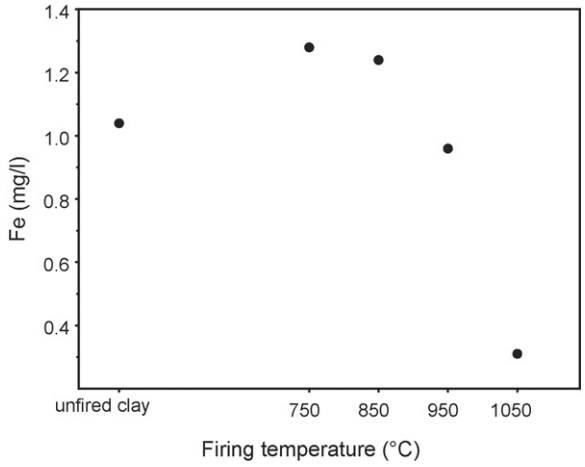

Fig. 7. Dithionite soluble iron concentration, as determined by OES-ICP *vs.* firing temperature.

As the CO_3^{2-} vibration signal is influenced by perturbations in the crystalline field,[30] the observed calcite pattern (Fig. 3b) may be attributed to recrystallisation of a primary fine-grained micritic, possibly partially substituted, calcite. In addition, the vicinity of the CO_3^{2-} stretching band of dolomite – which is located at 1448 cm^{-1} in the raw material – may also influence calcite peak position.

Comparing the mineral assemblage observed in the fired samples and that predicted from the ACS (Al_2O_3–CaO + MgO–SiO_2) diagram, by projecting the bulk chemical composition of the starting clay (Fig. 4), disequilibrium conditions apparently arise, since periclase and diopside also occur, as well as quartz, gehlenite and anorthite. Instead, local equilibrium conditions may have controlled nucleation and growth of mineral phases, which could not equilibrate with the bulk chemical composition due to sluggish diffusion and the relatively short residence time of firing.[31,1]

As regards changes in Fe-bearing mineral phases as revealed by Mössbauer spectra, the most evident effect on Fe sites at low T_f was a progressive Fe(II) oxidation (Fig. 5a). Above 400 °C, Fe was completely oxidised and distributed within two different paramagnetic Fe(III) sites (A and B). A further increase in T_f caused a progressive decrease in the relative area of site A and an increase in that of site B, probably due to the formation of iron oxides after decomposition of silicates (Fig. 5a). A magnetic signal became evident for $T_f > 500$ °C, and was attributed to an Al-substituted hematite on the basis of hyperfine parameters.[23] This signal progressively increased up to $T_f = 950$ °C and then rapidly decreased for further temperature increase (Fig. 5a).

Quadrupole splitting, which provides a measure of site asymmetry, significantly increased in both paramagnetic sites up to 600 °C (Fig. 5b), suggesting progressive site distortion caused by dehydroxylation of silicates and associated lattice collapse. Above 850 °C, quadrupole splitting rapidly decreased, coinciding with the growth of high-temperature silicates.

The 80 K spectra for samples fired at $T_f < 500$ °C were fitted using a paramagnetic Fe(III) site (A'), a paramagnetic Fe(II) site (C), and a magnetic sextet due to the contribution of nano-sized or sometimes larger oxide particles (Fig. 5c). This indicates that Fe(II) actually persisted at slightly higher temperatures than those indicated by the RT spectra. In addition, the magnetic component was observed here throughout the T_f range, as well as in the starting clay, and progressively increased with T_f. According to this model, site B in the RT Mössbauer spectra derives from the overlap of paramagnetic species and a superparamagnetic oxide, the latter contributing more to the relative area of the site, in agreement with observed relative area variations with increasing T_f. The relative area of site A' also increased up to 750 °C, remained quite constant in the interval 750–850 °C, and then decreased

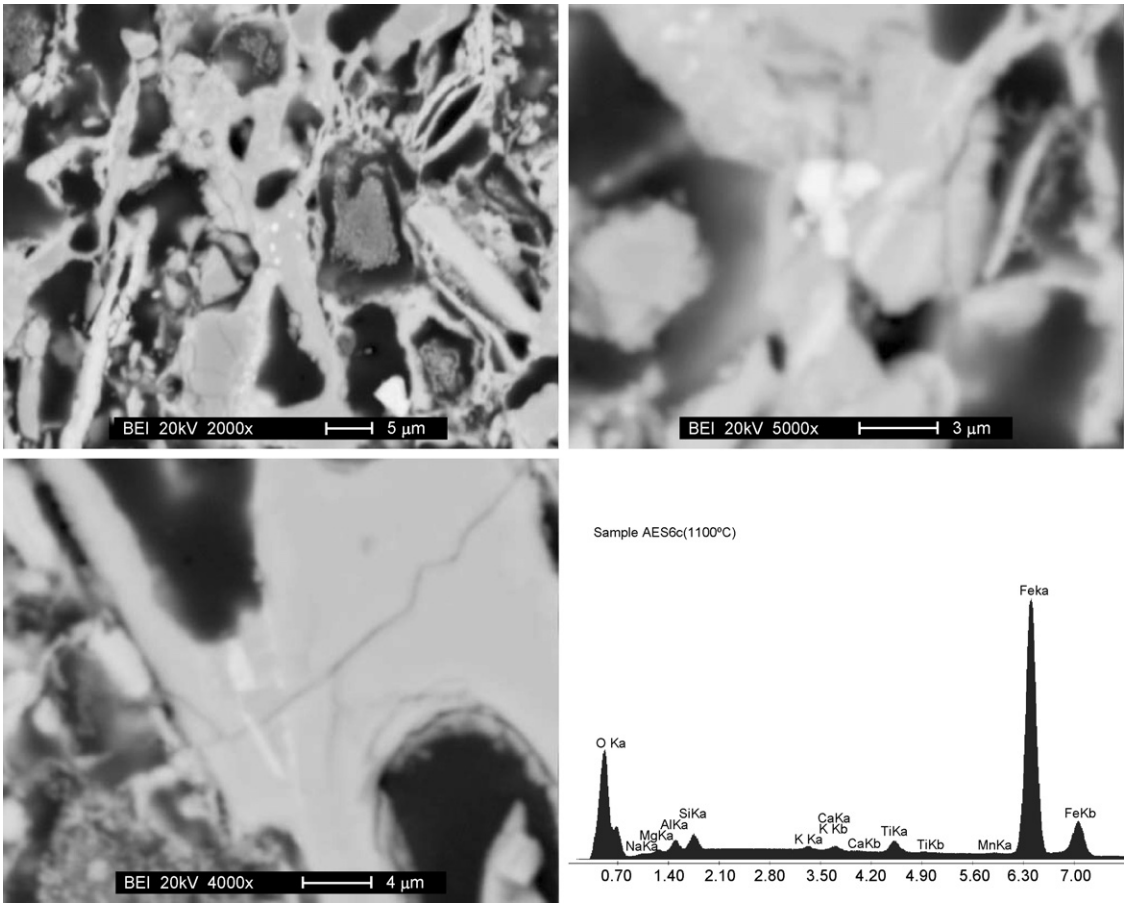

Fig. 8. Backscattered electron images of glass portion of ceramics hosting sub-micrometric hematite crystals with relative EDS spectrum.

above 850 °C, coinciding with an increase in the magnetic component.

4. Discussion

The combination of XRD, FT-IR and Mössbauer data provides some constraints on nucleation, growth and changes in iron oxides grain size in the firing of carbonate-rich clay. Complete oxidation of Fe(II) at about 500 °C coincides with chlorite decomposition, suggesting that iron oxidation is controlled by iron availability rather than oxidation efficiency. However, the 80 K Mössbauer spectra (Fig. 5c) indicate that iron remained in a paramagnetic site (A'), and that the magnetic fraction remained basically constant, coinciding with that originally present in the starting clay. This suggests that the decomposition of chlorite produced an amorphous phase rather than contributing to the nucleation of new mineral phases, in agreement with the increase in paramagnetic site distortion marked by the pattern of quadrupole splitting in Fig. 5b. Transformation of chlorite into an amorphous phase continued up to 700 °C, when chlorite reflections completely disappeared from the XRD patterns (Fig. 2), while the magnetic component in 80 K Mössbauer spectra continued to be constant. Therefore, the magnetic component detected in the RT Mössbauer spectra starting from 500 °C is probably related to coarsening of nano-sized oxide particles already present in the starting clay.

In addition, the following observations should be considered:

- The total magnetic fraction in the 80 K Mössbauer spectra started to increase from about 800 °C (Fig. 5c).
- This trend was not detected in the corresponding RT spectra (Fig. 5a).
- Carbonates completely decomposed between 750 and 850 °C (Fig. 2).
- Gehlenite and diopside crystallised between 750 and 900 °C (Fig. 2).
- Quadrupole splitting rapidly decreased above 850 °C (Fig. 5b).

These data suggest that decomposition of carbonates promoted rapid crystallisation of Ca-silicates at the expense of the amorphous phase. In this process, iron was released from the distorted paramagnetic site of the amorphous phase, partly forming new nano-sized hematite and partly being incorporated into paramagnetic sites in Ca-silicates.

This evolution of the magnetic component was also confirmed by the pattern of the magnetic ratio (MR), expressed as the magnetic over the total area of a spectrum (Fig. 6a). In the case of the RT Mössbauer measurements, MR represents the coarser-grained magnetic fraction, whereas in that of the 80 K spectra, MR refers to the total magnetic component – i.e., nano-sized and coarser-grained magnetic particles.

A measure of the variations in the superparamagnetic component with T_f may also be obtained by subtracting the coarse-grained magnetic contribution from the total oxide contribution (Fig. 6b). For $T_f < 400\,^{\circ}C$, no significant variations in the amount of superparamagnetic component were observed. The quadrupole shift in the 80 K spectrum slightly increased, from −0.27 mm/s in the starting clay to −0.16 mm/s at 400 °C, with a magnetic field value (51.3 T) compatible with Al-substituted hematite, suggesting that the original goethite underwent dehydroxylation.[32]

In the T_f interval 400–700 °C, the superparamagnetic component progressively decreased, suggesting grain coarsening, with little or no nucleation of new hematite. This evidence confirms the idea that the kinetics of silicate decomposition are sluggish with respect to crystal growth in this temperature interval, and that paramagnetic iron remains in a silicate-like structure within an amorphous phase. Above 750 °C, decomposition of carbonates and growth of gehlenite and diopside involve the amorphous phase, releasing iron, which nucleates into nano-sized hematite particles (Fig. 5c). However, the superparamagnetic component remained quite constant at low values up to 950 °C (Fig. 6b), indicating that nucleation and growth processes proceeded at the same rate. This may be explained by considering that several nano-sized hematite particles were probably concentrated within microdomains, each corresponding to a former chlorite flake, and they could therefore easily be reorganised into coarser-grained hematite crystals.

After illite had completely decomposed at 950 °C (Fig. 2), producing a glass, as suggested by Si–O stretching band broadening in the FT-IR spectra (Fig. 3a), the superparamagnetic component rapidly increased (Fig. 6b), indicating an increase in the amount of nano-sized *versus* coarser-grained hematite particles. These observations also indicate that the amorphous phase was involved in the melting process, producing a Fe-saturated glass, from which nano-sized hematite crystals precipitated. Low iron diffusion within the glass and short soaking time may have favoured nucleation and inhibited crystal growth.

In order to confirm this hypothesis, dithionite soluble iron was extracted from the starting clay and from samples fired at 750 °C, 850 °C, 950 °C and 1050 °C, respectively, and its concentration into the solution analysed by OES-ICP. It is well known that extraction efficiency depends on the dimensions and crystallinity of oxide particles, as well as on the nature of the matrix in which the oxides are embedded.[12] For example, efficiency in the extraction of dithionite soluble iron is severely compromised when nano-sized hematite particles are located within a glass. At 750 °C and 850 °C, the concentration of dithionite soluble iron was much higher than in the starting clay (Fig. 7), in agreement with the crystallisation of hematite during firing, whereas at $T_f \geq 950\,^{\circ}C$ it dramatically dropped. This is consistent with the growing difficulty in the extraction of iron from hematite increasingly located within a glass. Accordingly, high-magnification SEM backscattered images (Fig. 8) show that hematite crystals are mainly located within a glass at temperatures as high as 1050 °C and 1100 °C.

5. Conclusions

The nucleation, growth and grain size of hematite during firing in an oxidising atmosphere are strictly controlled not only by the availability of iron, but also by the structure and evolution of domains at the micro-scale. The thermal decomposition of Fe-rich sheet silicates such as chlorite produces an amorphous phase, which continues to retain iron in paramagnetic octahedral sites, inhibiting the crystallisation of hematite well above the disappearance of the relative reflections from the XRD pattern.

When carbonates are present in the clay, they decompose between 750 and 850 °C, and react with the amorphous phase to produce diopside and gehlenite. In these conditions, hematite is able to nucleate as nano-sized particles and grow within microdomains corresponding to former chlorite flakes. Some iron may also be accommodated in Ca-silicates, causing a rapid decrease in quadrupole splitting, due to progressive organisation of paramagnetic octahedral sites.

The decomposition of illite at 950 °C in the presence of CaO and residual amorphous matter produces a relatively Fe-rich silicate melt, which dramatically modifies the neighbourhoods of iron and determines radical changes in the evolution of hematite. Nano-sized hematite particles precipitate from the melt, increasing the superparamagnetic contribution, which progressively becomes dominant over the total magnetic component with increasing firing temperature, indicating that iron diffusion in the melt is low with respect to the applied soaking time, and insufficient to allow the growth of nano-sized hematite particles.

Therefore, changes in physical properties such as pottery colour seem to be related to the microstructural location and grain-size of hematite particles and to the presence of iron in glass rather than in Ca-silicate phases. The location of hematite within a glass significantly reduces its reactivity to hydroxylation and improves the durability of pottery to weathering.

Acknowledgements

We would like to thank Dr. Elena Campedello for the OES-ICP analysis. This work was carried out with the financial support of MIUR project PRIN 2005 no. 2005042574. We thank G. Walton for revising the English text.

References

1. Riccardi, M. P., Messiga, B. and Duminuco, P., An approach to the dynamics of firing. *Applied Clay Science*, 1999, **15**, 393–409.
2. Cultrone, G., Rodriguez-Navarro, C., Sebastian, E., Cazalla, O. and De La Torre, M. J., Carbonate and silicate phase reactions during ceramic firing. *European Journal of Mineralogy*, 2001, **13**, 621–634.
3. Duminuco, P., Messiga, B. and Riccardi, M. P., Firing process of natural clays: some microtextures and related phase composition. *Thermochimica Acta*, 1998, **321**, 185–190.
4. Dondi, M., Ercolani, G., Fabbri, B. and Marsigli, M., Chemical composition of melilite formed during the firing of carbonate-rich and iron-containing ceramic bodies. *Journal of American Ceramic Society*, 1999, **82**, 465–468.
5. González-García, F., Romero-Acosta, V., García-Ramos, G. and González-Rodríguez, M., Firing transformations of mixtures of clays containing illite, kaolinite and calcium carbonate used by ornamental tile industries. *Applied Clay Science*, 1990, **5**, 361–375.

6. Duminuco, P., Riccardi, M. P., Messiga, B. and Setti, M., Modificazioni tessiturali e mineralogiche come indicatori della dinamica del processo di cottura di manufatti ceramici. *Ceramurgia*, 1996, **26**, 281–288.
7. Jordán, M. M., Boix, A., Sanfeliu, T. and de la Fuente, C., Firing transformations of cretaceous clays used in the manufacturing of ceramic tiles. *Applied Clay Science*, 1999, **14**, 225–234.
8. Carretero, M. I., Dondi, M., Fabbri, B. and Raimondo, M., The influence of shaping and firing technology on ceramic properties of calcareous and non-calcareous illitic-chloritic clays. *Applied Clay Science*, 2002, **20**, 301–306.
9. Bauluz, B., Mayayo, M. J., Fernández-Nieto, C., Cultrone, G. and González López, J. M., Assessment of technological properties of calcareous and non-calcareous clays used for the brick-making industry of Zaragoza (Spain). *Applied Clay Science*, 2003, **24**, 121–126.
10. Cultrone, G., Sebastián, E. and de la Torre, M. J., Mineralogical and physical behaviour of solid bricks with additives. *Construction and Building Materials*, 2005, **19**, 39–48.
11. Orts, M. J., Escardino, A., Amorós, J. L. and Negre, F., Microstructural changes during the firing of stoneware floor tiles. *Applied Clay Science*, 1993, **8**, 193–205.
12. Khalfaoui, A., Kacim, S. and Hajjaji, M., Sintering mechanism and ceramic phases of an illitic-chloritic raw clay. *Journal of the European Ceramic Society*, 2006, **26**, 161–167.
13. Maritan, L., Nodari, L., Mazzoli, C. and Russo, U., Second Iron Age grey pottery from Este (North-eastern Italy): provenance and production technology. *Applied Clay Science*, 2005, **29**, 31–44.
14. Maritan, L., Nodari, L., Mazzoli, C., Milano, A. and Russo, U., Influence of firing conditions on ceramic products: experimental study on clay rich in organic matter. *Applied Clay Science*, 2006, **31**, 1–15.
15. Molera, J., Pradell, T. and Vedrell-Saz, M., The colours of Ca-rich ceramic paste: origin and characterization. *Applied Clay Science*, 1998, **13**, 187–202.
16. Maniatis, Y., Simopoulos, A. and Kostikas, A., Mössbauer study of the effect of calcium content on iron oxide transformations in fired clays. *Journal of American Ceramic Society*, 1981, **64**, 263–269.
17. Mackenzie, K. J. D., A Mössbauer study of the high-temperature reactions of iron oxides with calcium silicates. *Journal of Materials Science*, 1982, **17**, 1834–1842.
18. Wagner, F. E. and Wagner, U., Mössbauer spectra of clays and ceramics. *Hyperfine Interactions*, 2004, **154**, 35–82.
19. Oh, S. J. and Cook, D. C., Mössbauer effect determination of the relative recoilless fraction for iron oxide. *Journal of Applied Physics*, 1999, **85**, 329–332.
20. Mehra, O. P. and Jackson, M. L., Iron oxide removal from soils and clays by a dithionite-citrate system buffered with sodium bicarbonate. *Clays & Clay Minerals*, 1960, **7**, 317–327.
21. Mackenzie, R. C., *The Differential Thermal Investigation of Clay*. Mineralogical Society, London, 1957.
22. Stucki, J. W. and Bish, D. L., *Thermal Analysis in Clay Science*. Clay Minerals Society, 1990.
23. Murad, E. and Johnston, J. H., In *Iron Oxide and Hydroxides. Mössbauer Spectroscopy Applied to Inorganic Chemistry*, ed. G. J. Long. Plenum Press, New York, 1987.
24. Dondi, M., Ercolani, G., Guarini, G., Marsigli, M. and Venturi, I., Evoluzione della microstruttura durante la cottura rapida di impasti per piastrelle porose. *Ceramurgia*, 1995, **25**, 301–314.
25. De Benedetto, G. E., Laviano, R., Sabbatini, L. and Zambonin, G. P., Infrared spectroscopy in the mineralogical characterisation of ancient pottery. *Journal of Cultural Heritage*, 2002, **3**, 177–186.
26. Deer, W. A., Howie, R. A. and Zussman, J., *An Introduction to Rock Forming Minerals*. Prentice Hall, London, 1992.
27. Boynton, R. S., *Chemistry and Technology of Lime and Limestone* (*2nd ed.*). Wiley, New York, 1980.
28. Shoval, S., Using FT-IR spectroscopy for study of calcareous ancient ceramics. *Optical Materials*, 2003, **24**, 117–122.
29. Maritan, L., Mazzoli, C. and Freestone, I., Modelling changes in mollusc shell internal micro-structure during firing: implication for temperature estimate in shell-bearing pottery. *Archaeometry*, 2007, **49**, in press.
30. Engin, B., Demirtas, H. and Eken, M., Temperature effects on egg shells investigated by XRD, IR and ESR techniques. *Radiation Physics and Chemistry*, 2006, **75**, 268–277.
31. Heimann, R. B., Assessing the technology of ancient pottery: the use of ceramic phase diagrams. *Archaeomaterials*, 1989, **3**, 123–148.
32. Murad, E. and Wagner, U., Clays and clay minerals: the firing process. *Hyperfine Interactions*, 1998, **117**, 337–356.